1. Simulation of Glacial Background Climate

Globally averaged surface air is 3 K cooler than in the pre-industrial simulation. This is less than the 4-7 K cooling estimated for the Last Glacial Maximum [1], but consistent with intermediate glacial conditions during Marine Isotope Stage 3 (60-25 ka before present). Physically forced changes in marine and terrestrial carbon cycles result in a modeled glacial atmospheric CO_2 concentration of 255 ppmv, about 25 ppmv lower than the present-day solution, but significantly higher than the observed glacial concentrations (180-220 ppmv). This discrepancy suggests that processes not included in the model, such as changes in aeolian iron supply and/or interactions with ocean sediments, are important on those longer glacial-interglacial time scales [2]. Here we assume that these processes are not important on millennial time scales.

2. N_2O Calculation

The model predicts a global pre-industrial marine N_2O production of 3.7 Tg N/ yr, which is at the lower end of the range of observation based estimates [3,4]. In the 'glacial' simulation, oceanic N_2O production is decreased by 22% to 2.9 Tg N/yr due to increased oxygen solubility in colder water, consistent with marine sediment evidence. Terrestrial N_2O production, which is a poorly-understood function of soil moisture and oxygenation, is not explicitly modeled. Instead, to calculate the effect of changes in marine production on atmospheric N_2O concentrations we assume a constant terrestrial source twice the size of the oceanic source at year 0 (as estimated for present day), a constant atmospheric lifetime of 120 years, initial N_2O concentrations of 250 ppbv, and an instantaneous balance between oceanic and terrestrial sources and the atmospheric sink. Since we calculate atmospheric N_2O offline its changes do not affect modeled climate (in contrast to CO_2 changes). This is warranted because the radiative effect of the resulting N_2O changes is small.

3. Age scales of Figure 2

The age scales of Byrd and Taylor Dome (Figure 2) were previously synchronized to the GISP2 age scale by *Ahn and Brook* [5] using the sequence of rapid changes in CH_4 concentrations observed in all ice cores. In order to compare these Antarctic records to the Greenland $\delta^{18}O$ and N_2O of *Fluckiger et al.* [6], and the $\delta^{18}O$ of [7], which are on the comparable NGRIP and EDC3 age scales, respectively, the rapid CH_4 increase at the start of D-O interstadial #12 was used as a tie-point. This shifted the GISP2 ages by a uniform increment of 1.8 ky.

4. Uncertainty in Land Carbon Simulations

Prior studies have shown that the response of C_L is model-dependent, with pronounced sensitivities to atmospheric forcing and the background climate [8-11], therefore remaining uncertain. In contrast, the relationship between pCO_2 and Southern Ocean temperatures through multiple D-O events is very regular, giving strong support to our oceanic mechanism, which is relatively insensitive to background climate state. The response time of C_L to the rapid atmospheric forcing (temperature and precipitation changes) is in the order of decades to centuries [8-11] and thus much shorter than that of the ocean. (The millennial variability of C_L in Figure S1 is due to changes in atmospheric CO_2 via carbon fertilization and thus an indirect consequence of marine carbon changes.) Thus, the

millennial time scale of the observed pCO_2 variations indicates an oceanic mechanism, although other slowly varying processes such as changes in weathering or shallow-water carbonate sedimentation could also be significant. Our model does not simulate wind changes and associated precipitation variations. Related vegetation changes, particularly in the tropics due to shifts of the intertropical convergence zone, are therefore not represented in our simulations.

5. A Note on the Relation Between the Duration of D-O Oscillations and the Amplitude of the N_2O and CO_2 Variations

Fundamentally, both for N_2O and CO_2, the system can be approximated as a damped, forced harmonic oscillator (at high friction). See any textbook on mechanics as reference, we used [12]. We assume the D-O oscillations act as an idealized harmonic forcing with period T. In this case a relation between the response amplitude ($A \sim (1/\tau^2 - 1/T^2)^2 + g/T^2)^{-0.5}$, g represents friction) and T is expected if the response time (τ) of the system (for N_2O the upper ocean oxygen inventory and for CO_2 the preformed nutrient inventory) is similar to (but slightly larger than) the half-period of the forcing ($T_{1/2}=T/2$). If $\tau >> T_{1/2}$ the system has not enough time to respond to the high frequency forcing, the amplitude will be zero (independent of $T_{1/2}$). Typically the amplitude will be very small if $\tau \geq 3T$. On the other hand, if $\tau << T_{1/2}$ the system has always enough time to respond with the full amplitude and, again, the amplitude does not depend on $T_{1/2}$. Only if $\tau \sim T_{1/2}$ ($t>T_{1/2}$ for most cases) the amplitude depends on $T_{1/2}$ and it will strengthen with increasing $T_{1/2}$, regardless of the phase of the oscillation. The response time for N_2O deduced from the model is $\tau_{N2O} \sim 500$ years, whereas for CO_2 it is $\tau_{CO2} \sim 2000$ years (see Fig. 1, black lines). Thus, for N_2O we would expect increasing amplitudes for D-O oscillations with periods of 167-1000 years, whereas for CO_2 such a dependency can be expected for D-O oscillations with periods of 667-4000 years.

The relation between amplitude and duration of the D-O oscillations is independent on the phase of the oscillation. As such our approach to plot the amplitude of the N2O decrease following an interstadial to stadial transition (inset in Fig. 2) is expected to yield very similar results as the approach by ref (11) to plot the amplitude of the N2O increase following a stadial to interstadial transition (their Fig. 6).

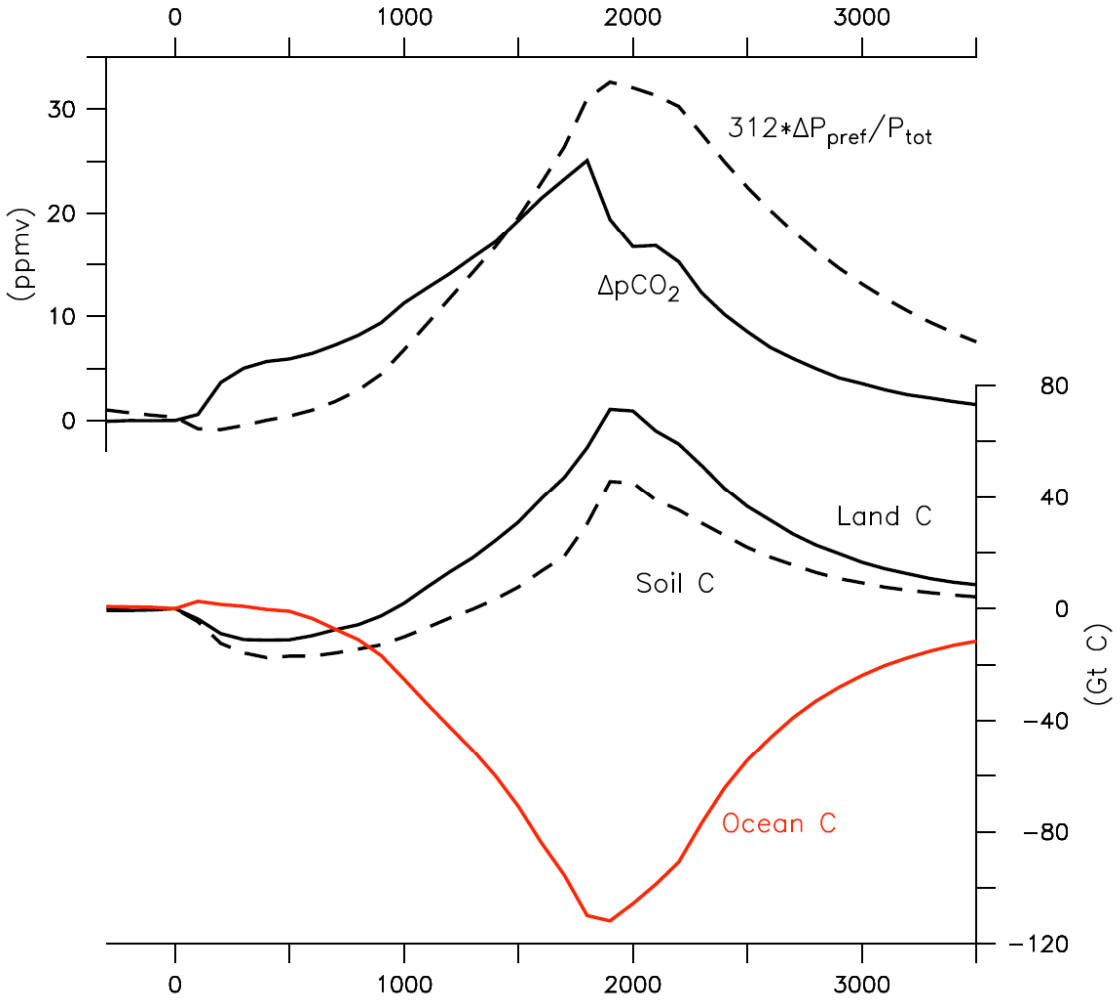

Figure S1: Time series of changes in carbon inventories for the simulation shown as red lines in Fig. 1). Top: atmospheric CO_2 (ΔpCO_2) simulated by the complex model (solid) compared to the simple theory (dashed). Changes in atmospheric CO_2 are due to changes in land carbon (C_L) and ocean carbon (C_O) inventories, $\Delta pCO_2 = - \Delta C_L - \Delta C_O$. Bottom: changes in C_L (black solid) and C_O (red) (2.13 Gt C = 1 ppmv). Changes in land carbon are due to changes in soil carbon (dashed) and vegetation carbon (difference between black solid and dashed lines). The initial small (5 ppmv) but rapid (within 250 years) increase of atmospheric CO_2 is due to a decrease in soil carbon on land. This response in the land carbon explains the difference between the simulated atmospheric CO_2 changes and the theory. The rapid initial decrease in soil carbon is caused by a decrease in boreal forest in northeastern Europe and Siberia (not shown) and the rapid drop in atmospheric CO_2 at year 1800 is due to an abrupt arrest in the decrease of the oceanic carbon inventory, whereas the land carbon continues its increase. Thus both changes in land and ocean carbon inventories are clearly important for the atmospheric CO_2 evolution, but the ocean dominates on longer (multi-centennial to millennial) time scales.

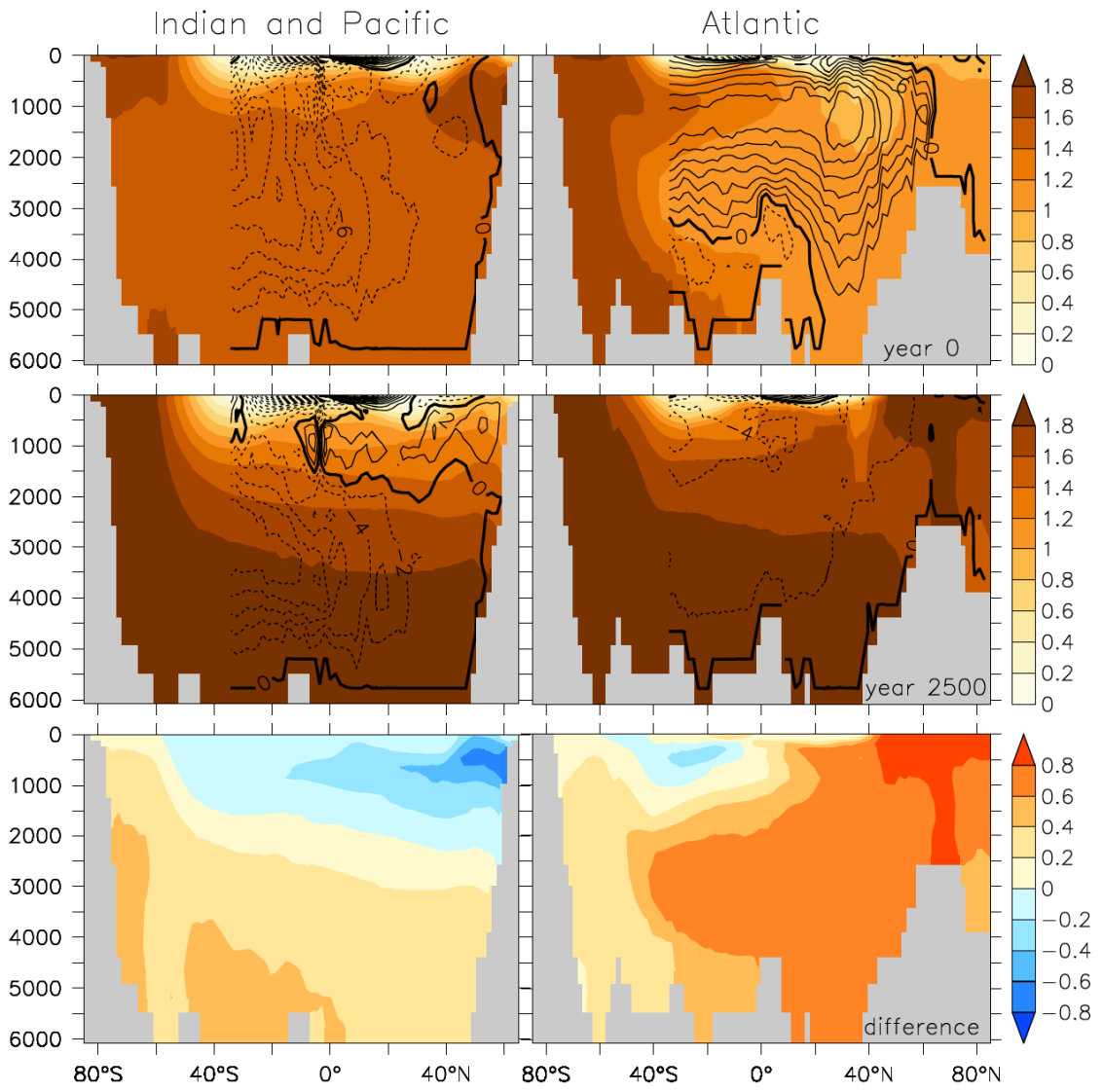

Figure S2: Preformed phosphate concentrations in mmol/m^3 (color scale) zonally averaged in the Indian and Pacific oceans (left) and Atlantic (right) as a function of latitude (horizontal axis) and depth (in m, vertical axis) for the simulation shown as black lines in Fig. 1. The top row is the state at year 0 with a strong overturning in the Atlantic. Isolines show the zonally integrated flow as represented by the Eulerian streamfunction with an isoline difference of 2 Sv (1 Sv = 10^6 m^3/s). Solid lines (positive streamfunction) show clockwise flow, dashed lines indicate counter-clockwise flow. The downwelling of nutrient poor surface waters in the northern North Atlantic leads to low preformed nutrient concentrations at the depth of southward flowing North Atlantic Deep Water (1.5 – 3.5 km). The center row shows the state 2500 years after NADW formation stopped. The bottom row depicts the differences (year 2500 minus year 0). The reduction of NADW leads to increased preformed nutrient concentrations in the North Atlantic and in the deep Indian and Pacific oceans below 2000 m and to decreases in the upper North Pacific ocean.

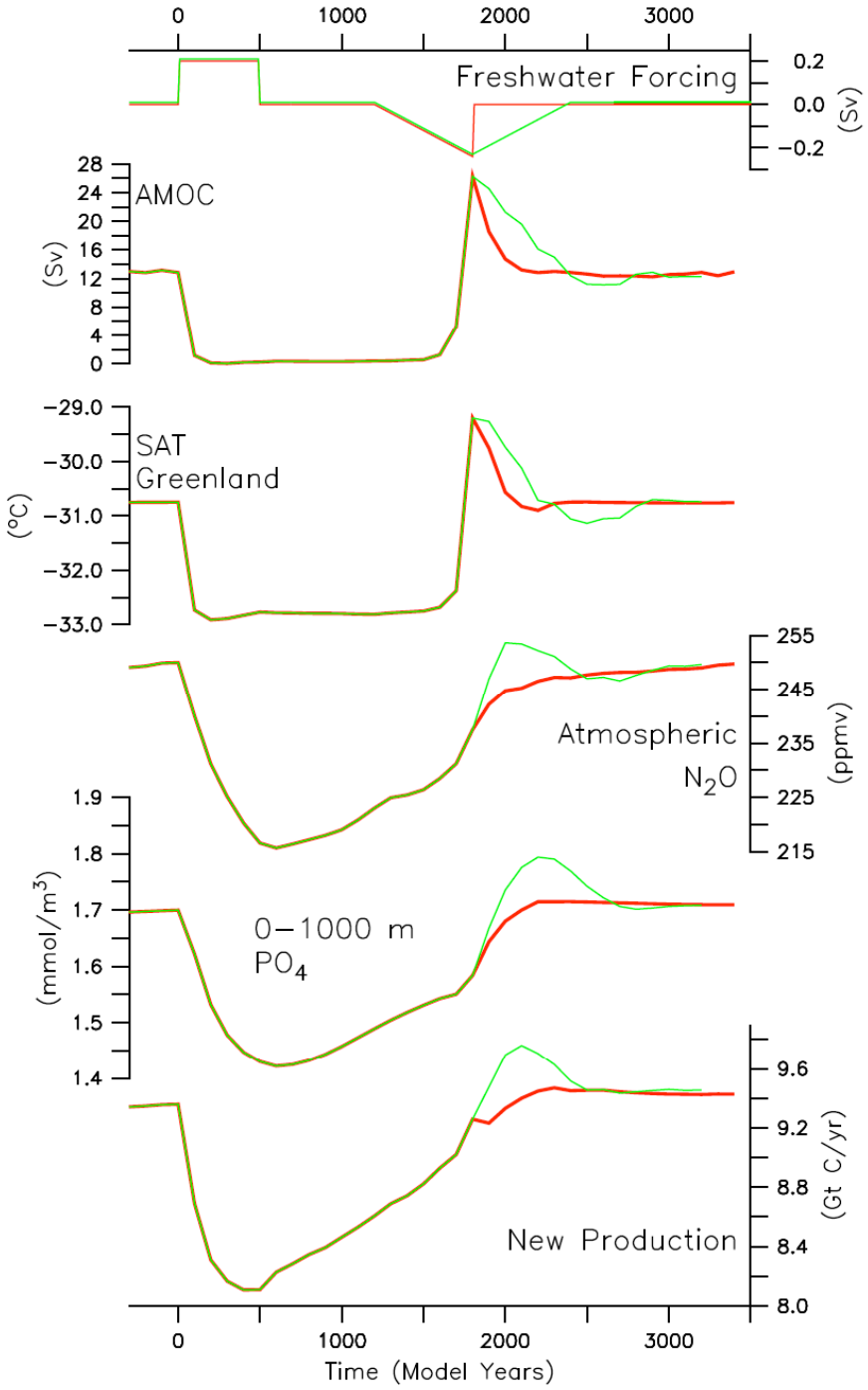

Figure S3: Sensitivity of AMOC, Greenland temperature, N_2O, globally averaged upper ocean (0-1000 m) phosphate concentrations and globally integrated new production to different freshwater forcing functions. The red lines show the same simulation as they show in Fig. 1. The green lines show the influence of a slight change in the forcing (top panel). In this case the forcing decreases gradually instead of abruptly after year 1800. This leads to a post-stadial peak in N_2O concentrations followed by a gradual decrease, consistent with the observations (Fig. 2).

REFERENCES

1 Jansen, E. et al., in *Climate Change 2007: The Physical Science Basis. Contribution of Working Group I to the Fourth Assessment Report of the Intergovernmental Panel on Climate Change*, edited by S. Solomon, D. Qin, M. Manning, Z. Chen, M. Marquis, K.B. Averyt, M. Tignor and H.L. Miller (Cambridge University Press, Cambridge, United Kingdom and New York, NY, USA, 2007).

2 Brovkin, V., Ganopolski, A., Archer, D., and Rahmstorf, S., Lowering of glacial atmospheric CO2 in response to changes in oceanic circulation and marine biogeochemistry. *Paleoceanogr.* 22, Pa4202 (2007).

3 Nevison, C., Butler, J. H., and Elkins, J. W., Global distribution of N2O and the Delta N2O-AOU yield in the subsurface ocean. *Glob. Biogeochem. Cycles* 17, 1119 (2003).

4 Hirsch, A. I. et al., Inverse modeling estimates of the global nitrous oxide surface flux from 1998-2001. *Glob. Biogeochem. Cycles* 20, Gb1008 (2006).

5 Ahn, J. and Brook, E. J., Atmospheric CO2 and climate from 65 to 30 ka BP. *Geophys. Res. Lett.* 34, L10703 (2007).

6 Fluckiger, J. et al., N2O and CH4 variations during the last glacial epoch: Insight into global processes. *Glob. Biogeochem. Cycles* 18, GB1020 (2004).

7 EPICA, One-to-one coupling of glacial climate variability in Greenland and Antarctica. *Nature* 444, 195-198 (2006).

8 Scholze, M., Knorr, W., and Heimann, M., Modelling terrestrial vegetation dynamics and carbon cycling for an abrupt climatic change event. *Holocene* 13, 327-333 (2003).

9 Obata, Atsushi, Climate-Carbon Cycle Model Response to Freshwater Discharge into the North Atlantic. *J. Clim.* 20, 5962-5976 (2007).

10 Menviel, L., A. Timmermann, A. Mouchet, and O. Timm, Meridional reorganizations of marine and terrestrial productivity during Heinrich events. *Paleoceanogr.* 23, PA1203 (2008).

11 Kohler, P., Joos, F., Gerber, S., and Knutti, R., Simulated changes in vegetation distribution, land carbon storage, and atmospheric CO2 in response to a collapse of the North Atlantic thermohaline circulation. *Clim. Dyn.* 25, 689-708 (2005).

12 Kuypers, F., *Klassische Mechanik*. (VCH Verlagsgesellschaft, Weinheim, Germany, 1989).